© 2020. Published by The Company of Biologists Ltd | Journal of Cell Science (2020) 133, jcs246330. doi:10.1242/jcs.246330

RESEARCH ARTICLE

Investigating cell cycle-dependent gene expression in the context of nuclear architecture at single-allele resolution

Shivnarayan Dhuppar* and Aprotim Mazumder*

ABSTRACT

Nuclear architecture is the organization of the genome within a cell nucleus with respect to different nuclear landmarks such as the nuclear lamina, nuclear matrix or nucleoli. Recently, nuclear architecture has emerged as a major regulator of gene expression in mammalian cells. However, studies connecting nuclear architecture with gene expression are largely population-averaged and do not report on the heterogeneity in genome organization or gene expression within a population. In this report we present a method for combining 3D DNA fluorescence *in situ* hybridization (FISH) with single-molecule RNA FISH (smFISH) and immunofluorescence to study nuclear architecture-dependent gene regulation on a cell-by-cell basis. We further combine our method with imaging-based cell cycle staging to correlate nuclear architecture with gene expression across the cell cycle. We present this in the context of the cyclin-A2 (*CCNA2*) gene, which has known cell cycle-dependent expression. We show that, across the cell cycle, the expression of a *CCNA2* gene copy is stochastic and depends neither on its sub-nuclear position – which usually lies close to nuclear lamina – nor on the expression from other copies of the gene.

This article has an associated First Person interview with the first author of the paper.

KEY WORDS: Cell cycle, 3D nuclear architecture, Central dogma, DNA fluorescence *in situ* hybridization, Single-molecule RNA fluorescence *in situ* hybridization, Cyclin-A2, Nuclear lamina, Immunofluorescence

INTRODUCTION

Life at the cellular level is the result of the coordinated efforts of molecular machinery inside a cell brought about by timely expression of genes at mRNA and protein levels as posited by the central dogma of molecular biology (Crick, 1970). A cell achieves this by regulating genes at various stages of their expression – from the transcription of genes to the translation of their respective mRNAs and eventual degradation of the gene products (Day and Tuite, 1998; Wray et al., 2003; Zhao et al., 2017). Many of these effectors of gene regulation can be linked to two important factors: nuclear architecture and the cell cycle (Misteli, 2001; Sadasivam and DeCaprio, 2013). The cell cycle encompasses the complete gamut of processes by which a single cell divides into two daughter cells. This implies that almost all cellular events or attributes have to be coordinated with the cell cycle to ensure proper cell division – even the nuclear architecture (Cooper, 2000; Finn and Misteli, 2019; Probst et al., 2009). Nuclear architecture is the organization of the genome inside a cell nucleus with respect to nuclear compartments such as the nuclear lamina or heterochromatin. It can play a key role in determining the gene expression pattern in a cell and hence the cellular identity, as proposed by the topological model of gene regulation (TMGR) (Cremer and Cremer, 2001). The TMGR hypothesizes that: (1) spatial positioning of a gene with respect to chromosomal locations such as centromeres can affect the transcription of that gene, and (2) differentiating cells develop a pattern of gene positions with respect to nuclear compartments (such as the nuclear lamina, heterochromatin or interchromatin compartments) that defines patterns of gene expression and hence the eventual identities of those cells (Cremer and Cremer, 2001). There have been a number of studies supporting the TMGR but most of them lacked either single-cell resolution or the ability to interrogate gene position and expression at the same time in the same cells (Ernst et al., 2011; Fullwood et al., 2009; Morey et al., 2007, 2009). Single-cell-level studies on nuclear architecture-dependent gene expression have been elusive because they require the combination of immunofluorescence-based detection of proteins with fluorescent *in situ* hybridization (FISH)-based detection of gene positions and mRNAs while also preserving the 3D nuclear architecture of the cell. The existing methods for RNA FISH and 3D DNA FISH are incompatible because the steps involved in either can affect the detection of the other adversely.

Here we present a simple and reliable way to combine DNA FISH with single molecule RNA FISH (smFISH) and immunofluorescence while also preserving the 3D nuclear architecture of a cell. We further link it with a microscopy-based cell cycle staging method developed previously (Dhuppar and Mazumder, 2018) to study cell cycle-dependent changes in nuclear architecture and gene expression on a cell-by-cell basis. In particular, we investigate how the positioning of the cyclin-A2 (*CCNA2*) gene with respect to the nuclear lamina correlates with the known cell cycle-dependent expression of the gene.

The ease of the technique presented here, combined with the depth of the analyses, makes this method a useful tool in addressing various questions pertaining to the cell cycle, nuclear architecture and gene expression at a single-cell resolution.

RESULTS

Combined DNA FISH, smFISH and immunofluorescence in three-dimensionally intact nuclei

Genome organization has previously been shown to be involved in the regulation of gene expression. Most of these studies either rely on bulk biochemical assays for measuring expression (Thomson et al., 2004) or involve sequential FISH-based labeling and imaging

TIFR Centre for Interdisciplinary Sciences, Tata Institute of Fundamental Research Hyderabad, 36/P, Gopanpally, Serlingampally Mandal, Hyderabad 500046, Telangana, India.

*Authors for correspondence (shuppar@gmail.com; aprotim@tifrh.res.in)

S.D., 0000-0001-8772-1721; A.M., 0000-0002-3443-3010

Handling Editor: Maria Carmo-Fonseca
Received 13 March 2020; Accepted 10 May 2020

Journal of Cell Science

Journal of Cell Science (2020) 133, jcs246330. doi:10.1242/jcs.246330

of mRNA and the gene of interest – this relies heavily on the ability to mark and identify the same cells between the two steps (Clemson et al., 2009; Lomvardas et al., 2006; Morey et al., 2009). Recent years have seen the development of smFISH methods that yield absolute transcript counts on a cell-by-cell basis, unlike standard RNA FISH where only relative intensities are measured (Raj et al., 2006, 2008; Zenklusen et al., 2008). Although there have been previous studies investigating mRNA localization inside the cell (Buxbaum et al., 2015) or transcription in the context of nuclear architecture that combined DNA and RNA FISH (Clemson et al., 2009; Hall et al., 2002, 2014; Jiang et al., 2013; Lomvardas et al., 2006; Morey et al., 2009; Pageau et al., 2007), fewer attempts have been made to combine 3D DNA FISH with smFISH. The difficulty in combining DNA FISH with RNA FISH or immunofluorescence stems from the fact that DNA FISH involves harsh treatments, such as acid- or formamide-based DNA denaturation, which can adversely interfere with the subsequent detection of proteins or RNAs inside a cell (Morey et al., 2007; Zhang et al., 2007). Furthermore, the ethanol dehydration involved in such procedures destroys the 3D architecture of the cells – which are more than 50% water – by flattening them out. The organelle most affected by such dehydration would be the cell nucleus, whose water content can be as high as 85% (Century et al., 1970). This makes it difficult to combine the three assays while also minimizing distortions to nuclear architecture. Additionally, the existing protocols for 3D DNA FISH involve steps such as nitrogen freeze-thaw cycles, which add another layer of difficulty to the problem (Bienko et al., 2013; Bolland et al., 2013).

We started out by first standardizing a protocol for 3D DNA FISH devoid of conventional difficulties. We realized that the major and perhaps the only factor affecting the 3D nuclear architecture of a cell in a conventional 2D DNA FISH protocol is ethanol dehydration. We discovered that the loss in efficiency of probe hybridization due to omission of ethanol dehydration can be compensated for by having longer hybridization times (>40 h). The resulting protocol, in fact, is largely similar to a conventional 3D DNA FISH protocol if nitrogen freeze-thaw cycles are removed.

Once the protocol for 3D DNA FISH was standardized, the next step was to determine the order in which the three techniques can be performed for least interference among them. We observed that the order that gives the best result is the following: immunofluorescence followed by refixation with 4% paraformaldehyde, followed by DNA FISH and then smFISH for RNA. The order is especially important with regard to smFISH, where 20-nucleotide long oligomers are used as the hybridization probes. If not performed in the correct order, the high formamide concentration in the DNA FISH hybridization buffers can destroy all smFISH RNA signals.

Once standardized, we used the above technique to study how gene position inside the nucleus can be correlated with gene expression across the cell cycle in HeLa cells. We selected the *CCNA2* gene for our study due to its known cell cycle-dependent gene expression. We found that most cells had three copies of the *CCNA2* gene, which was consistent with the fact that HeLa cells are hypertriploid (Fig. 1A). We also observed that mRNA and protein expression levels of *CCNA2* were strongly correlated (Fig. 1A) and that the activity of two adjacent alleles, as inferred from the colocalization of smFISH and DNA FISH signals, could be very different – at least in 2D-projected images of nuclei (Fig. 1B).

To convert the above observations into quantifiable, comparable metrics we performed a quantitative 3D image analysis, as described below.

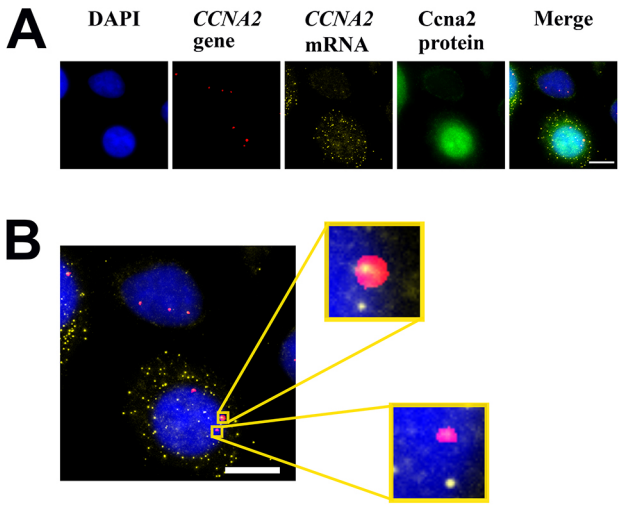

Fig. 1. Combined DNA FISH, smFISH and immunofluorescence. (A) Combined DNA FISH for gene position (red), smFISH for absolute mRNA counts (yellow) and protein immunofluorescence (green), for expression from the *CCNA2* gene. Nuclei are stained with DAPI (blue). The protein and mRNA expression are correlated; *CCNA2* mRNA and CCNA2 protein are both low in the upper cell and both high in the lower cell. For a detailed quantification of many cells across cell cycle phases see Fig. 3E. (B) Two adjacent copies of the *CCNA2* gene with different activity status are highlighted for the image shown in A. Enlarged images of the regions indicated by boxes are shown. Nascent transcripts are seen at one gene locus (top), but not at another (bottom). Three gene loci are seen in each nucleus as expected for HeLa cells. DAPI (blue) shows the full nuclei. The CCNA2 protein channel is not shown in B for clarity. Scale bars: 10 µm.

3D nuclear segmentation and cell cycle staging

Cells were first analyzed to quantify their DNA content in order to determine the cell cycle stage for each cell using a previously-developed module for imaging-based cell cycle determination (Dhuppar and Mazumder, 2018). Briefly, the workflow ran thus: the average-projected images from the DAPI channel were passed to a module that quantified the DNA content of individual nuclei in a field. Once DNA content was quantified, the 3D stack for each nucleus in a field was sent to another module that eliminated out-of-focus planes from the 3D stacks and segmented the nucleus in 3D, based on texture analysis (Fig. 2A). All 3D analyses were done in a cell-by-cell manner in order to reduce both the size of the images and the subsequent computer processing requirements. DNA FISH spots were also segmented in 3D, using another previously reported module (Dhuppar and Mazumder, 2018). Fig. 2B shows an example of one such 3D segmented nucleus and the segmented *CCNA2* alleles within (see also Movie 1). The nuclear volumes obtained from the above analysis compared well with those reported previously for HeLa cells (Fig. 2C) (Monier et al., 2000).

The 3D segmented nuclei and alleles thus obtained were then used to calculate distances from the centroid of an allele to the nuclear lamina and nuclear centroid in order to define a closeness metric, as discussed below.

The central dogma in the context of nuclear architecture and the cell cycle

The TMGR suggests that, upon differentiation, cells adopt the expression patterns of their differentiated states by defining a unique and reproducible pattern of gene positions with respect to different nuclear compartments such as the nuclear lamina, heterochromatin or interchromatin compartments (Cremer and Cremer, 2001).

Journal of Cell Science (2020) 133, jcs246330. doi:10.1242/jcs.246330

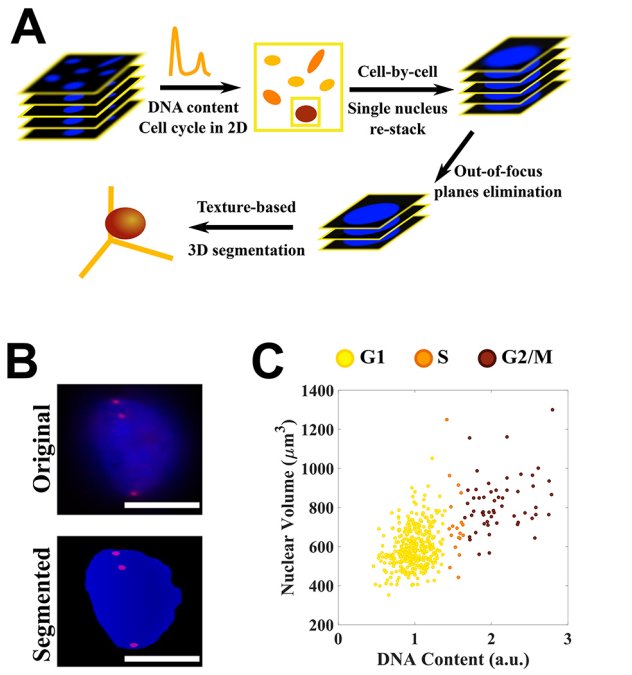

Fig. 2. 3D nuclear segmentation and cell cycle staging. (A) The workflow for 3D nuclear segmentation. Cells were first analyzed in 2D to determine their DNA content. Thereafter, a 3D stack for each nucleus was sent to an image processing module that removed out-of-focus light and segmented individual nuclei in 3D using texture-based analysis. (B) An example segmentation of a nucleus (blue) and the *CCNA2* gene copies within (red). (C) Volume measurements for HeLa cell nuclei, from the analysis described in A, indicating cells in different cell cycle stages. See Movie 1 for visualization of the 3D segmentation shown in B. Scale bars: 10 µm.

However, other studies have suggested that genes can make long extrusions out of their chromosome territories for their transcription (Morey et al., 2007; Osborne et al., 2004). This looping-out of genes for expression could be to avoid nuclear compartments such as the nuclear lamina or heterochromatin, which are generally associated with gene silencing (Finlan et al., 2008; Reddy et al., 2008; Wang et al., 2018). To determine which of the two models – the static TMGR model or the dynamic extrusion-based model – is true in the case of the *CCNA2* gene, we calculated the distances from the centroids of the three copies of *CCNA2* to the nuclear lamina and nuclear centroid, and then correlated them with expression of the *CCNA2* gene.

We observed that, although expression of *CCNA2* mRNA and CCNA2 protein peaked in the G2/M phases of the cell cycle (Fig. 3A,B), the mean of the absolute distances between the centroids of the gene copies and the nuclear lamina or the nuclear centroid did not change substantially across the cell cycle (Fig. 3C,D). Furthermore, we defined a closeness metric for the gene copies that could vary continuously between 0 and 1 – taking a value of 0 if the gene copy is at the nuclear centroid and 1 if it is at the lamina. We ranked the gene copies such that copy 1 corresponded to the gene copy with highest closeness value. We observed that the mean value of closeness in a cell did not correlate with the expression of *CCNA2* in terms of mRNA number or protein level (Fig. 3E). In fact, the mean closeness for the *CCNA2* gene did not vary much across the cell cycle, even though the expression was highly cell cycle-dependent (Fig. 3E).

The above observations strongly support the TMGR mode of gene regulation in the case of the *CCNA2* gene in the differentiated HeLa cancer cell line. However, the analysis is incomplete without information on the activity of the gene at a single-allele level. The following section discusses the position-dependent activity of *CCNA2* gene at a single-allele level.

Position-independent expression of *CCNA2* gene copies across the cell cycle

We measured the activity of a gene copy by determining the colocalization between smFISH and DNA FISH signals at a position in the nucleus in 3D. A cuboid just enveloping the gene spot was constructed and then was searched for the mRNA signal. If the cuboid contained at least one mRNA spot, then that gene copy was deemed as actively expressing. The expression metric thus defined was found to have high precision when verified against synthetic 3D images of similar spots (Fig. S1).

We observed that there was no obvious correlation between the position of a *CCNA2* allele and its expression across the cell cycle. However, there was a marginal increase in the percentage activity of the *CCNA2* copy farthest from nuclear periphery (Fig. S1C). As shown in Fig. 4, the expression of a gene copy depended little on its position relative to the lamina, or on the cell cycle stage. Gene copies could express in any cell cycle stage irrespective of subnuclear position – though overall mRNA levels are cell cycle dependent. We also investigated the number of *CCNA2* copies actively expressing in a cell and the corresponding total mRNA count. We found that the cells with higher mRNA counts, on average, had more gene copies with active transcription (Fig. S2). Interestingly, we found that cells with very low mRNA counts can have active expression from multiple gene copies, and cells with active expression from a single gene copy can have high mRNA counts. This illustrates the stochastic nature of gene activation via transcriptional bursts (Fig. S2) (Raj et al., 2006).

We also observed that two of the three alleles always remained close to the nuclear lamina (Fig. 4). This is striking, given that individual bona fide lamina-associated domains (LADs) can be randomized between two cell cycles (Nagano et al., 2017) even if the overall nuclear organization of chromosome territories can remain the same (Gerlich et al., 2003).

The above observations support the TMGR mode of action for *CCNA2* gene regulation, where the average position of the gene relative to the nuclear lamina varies little within the cell cycle even though expression of the gene – both at mRNA and protein levels – is highly cell cycle-dependent.

DISCUSSION

Nuclear architecture derives from the non-random organization of the eukaryotic genome in terms of its arrangement of chromosome territories and genes with respect to each other and to other nuclear landmarks, such as the nuclear lamina or nucleoli (Misteli, 2005). Nuclear architecture is involved in cell fate decisions during differentiation (Morey et al., 2007; Stadhouders et al., 2018, 2019) and has been shown to be tissue-specific (Parada et al., 2004). It is also implicated in the regulation of gene expression via association with different nuclear compartments such as the nuclear periphery, heterochromatin, euchromatin and interchromatin compartments (Holwerda and Laat, 2012; Sexton et al., 2007). Most of these studies are based on bulk biochemical assays that efficiently capture population-level changes in organization or expression but miss out on the cell-to-cell variability within a population. In fact, according to recent reports, there is a substantial level of heterogeneity in genome organization within a population, and at any given time only a small fraction of cells within a population harbor the

Journal of Cell Science (2020) 133, jcs246330. doi:10.1242/jcs.246330

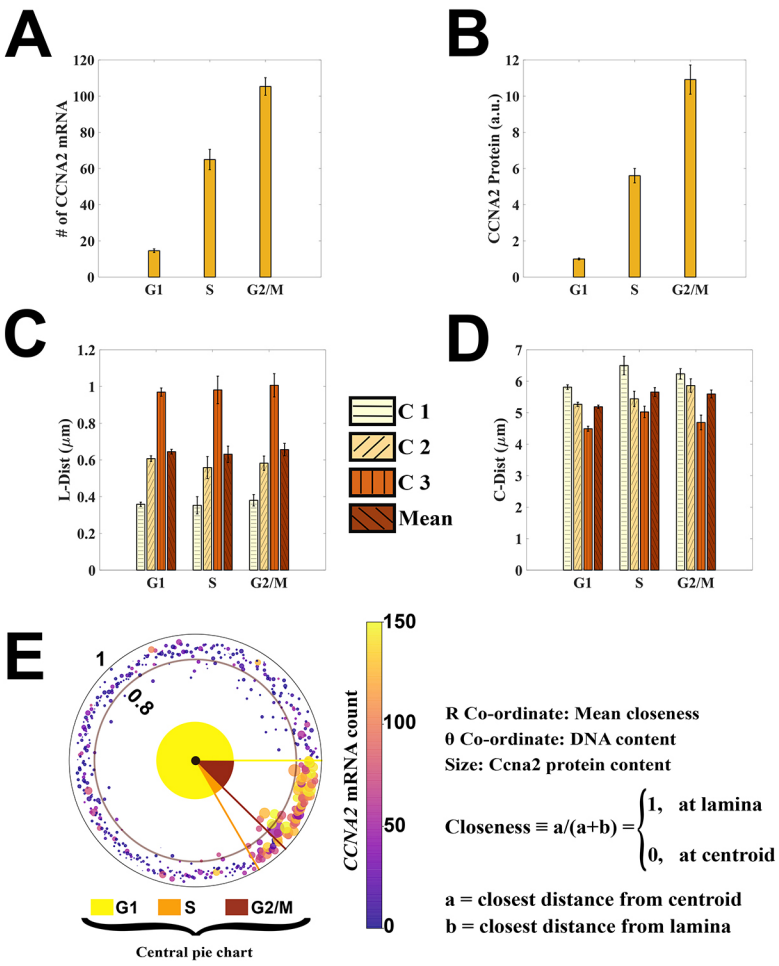

Fig. 3. The central dogma in the context of nuclear architecture and cell cycle. (A) Mean±s.e.m. *CCNA2* mRNA number peaks in the G2/M phase of the cell cycle. (B) Mean±s.e.m. CCNA2 protein levels also peak in the G2/M phase of the cell cycle. (C) Mean±s.e.m. distance of the three copies of *CCNA2* from the nuclear lamina in the three cell cycle phases. Gene copies are numbered according to their relative distances from the lamina (L-Dist) with C1 (copy 1) closest to the lamina followed by C2 and then C3. (D) Mean±s.e.m. distance of the three copies of *CCNA2* from the centroid of the nucleus (C-dist) in the three cell cycle phases. Gene copies are numbered as described in C. The means of the absolute values of both L-dist and C-dist do not change much across the cell cycle. (E) A polar plot representing the correlation between *CCNA2* expression and the mean closeness value for the three copies of *CCNA2* in a cell. Each spot on the graph is an individual cell, with spot color representing corresponding *CCNA2* mRNA count and spot size CCNA2 protein content. Although mRNA and protein expression for the *CCNA2* gene are well correlated across the cell cycle (both are high in S- and G2-phase cells), there is no obvious dependence of *CCNA2* expression on the average closeness of the gene copies to the lamina. The pie chart in the center of the plot represents the cell cycle distribution of the cell population. *n*=446 cells.

interactions captured at the population level (Finn and Misteli, 2019; Finn et al., 2019). This underscores the need for single-cell studies to capture nuclear architecture-dependent regulation of DNA processes in their entirety.

The existing methods to study 3D nuclear architecture and gene expression at single-cell resolution are incompatible with one another. Here we report a simple and efficient method to combine DNA FISH with smFISH and immunofluorescence that also preserves the 3D nuclear architecture of a cell. We further combined this with an imaging-based cell cycle staging process developed previously (Dhuppar and Mazumder, 2018) to study gene regulation in the context of nuclear architecture across the cell cycle for a cell cycle-regulated gene, *CCNA2*. DNA FISH methods that use extensive dehydration can cause flattening of the cell nucleus and loss of three-dimensional information. This is addressed by newer methods of 3D DNA FISH. Compared to other 3D DNA FISH techniques, our method is simpler and allows for multiplexing with smFISH for RNA and immunofluorescence for proteins. Although undoubtedly each of these methods have been performed many times in isolation by many groups, combining all three in the same cell provides direct insight into nuclear architecture-dependent gene expression.

We observed that the cell cycle dependence of *CCNA2* gene expression is hardly reflected in the average positioning of the *CCNA2* gene relative to the nuclear periphery (Fig. 3E). Interestingly, in contrast to previous studies associating positioning at the nuclear periphery with gene silencing (Finlan et al., 2008; Reddy et al., 2008; Wang et al., 2018), we observed that nuclear positioning of a *CCNA2* gene copy – which more often than not stays close to the nuclear periphery – matters little for its activity (Fig. 4; Fig. S1). Also, the number of *CCNA2* copies actively expressing in a cell does not reflect the overall mRNA count in that cell. There can be cells with very high mRNA count but fewer than two copies actively expressing, and vice versa. This demonstrates the stochastic nature of transcriptional bursts and gene regulation via the modulation of burst frequency (Li et al., 2018; Raj et al., 2006). This might also suggest a possible decoupling between the activities of different alleles within a nucleus where each is agnostic of the others' transcriptional status, unlike as reported recently in bacteria (Wang et al., 2019). The above observations further emphasize the importance of studying the heterogeneity in genome organization within a population at a single-cell resolution.

Finally, our method can potentially be combined with DNA FISH for chromosome territories. Thus, the experimental and analysis modules used in this study can easily be adapted to study the regulation of gene expression mediated by megabase-pair looping seen in differentiating stem cells (Chambeyron and Bickmore, 2004; Morey et al., 2009) or by short excursions of genes in differentiated cells to shared sites of transcription, also called 'transcription factories' (Osborne et al., 2004, 2007), on a cell-by-cell basis. Taken together, the technique presented here, along with the analysis modules, is a powerful tool to study nuclear architecture and nuclear architecture-dependent gene regulation across the cell cycle at single-cell resolution.

Journal of Cell Science (2020) 133, jcs246330. doi:10.1242/jcs.246330

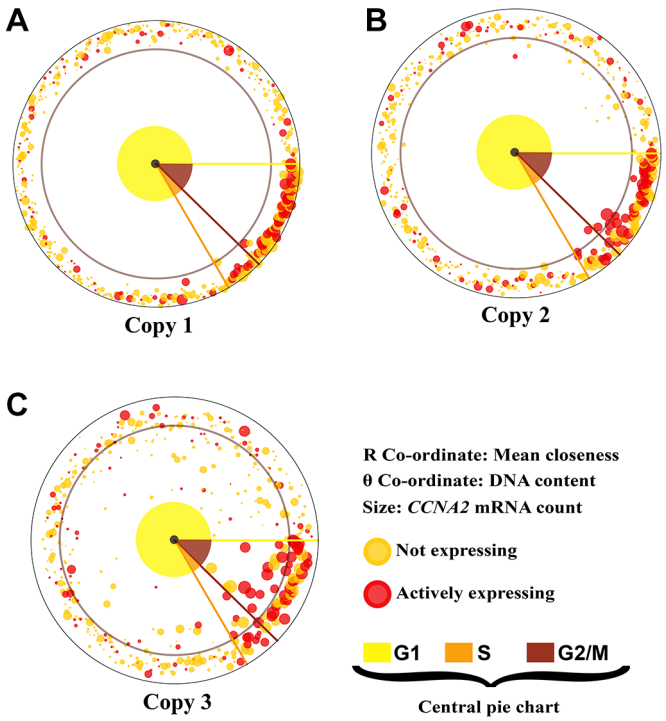

Fig. 4. Position-independent transcription of the *CCNA2* gene copies across the cell cycle. (A–C) Polar plots representing the individual position-dependent activity of the three copies of the *CCNA2* gene in a cell across the cell cycle. Gene copies are ranked by proximity to the lamina, with copy 1 the closest to the lamina. There is no correlation between the activity of a gene copy and its relative distance from the lamina, though a gene copy is more likely to express in the S or G2/M phases of the cell cycle. See also Figs S1, S2 for the cell cycle distribution of the number of *CCNA2* gene copies actively expressing in a cell. *n*=446 cells.

MATERIALS AND METHODS

Cell culture

HeLa cells were grown on ethanol-sterilized, poly-D-lysine-treated coverslips. The cell line was procured from the National Centre for Cell Science (NCCS), the national cell line repository of India. DMEM/F12 (Gibco) supplemented with 10% FBS (Gibco) without any antibiotic was used for cell culture. Cells were tested negative for bacterial contamination and mycoplasma. They were passaged every ∼4 d and were allowed to grow for at least 24 h before starting an experiment. Experiments were performed in conformity to the norms set out by the Institutional Biosafety Committee of TIFR Hyderabad.

Combined DNA FISH, smFISH and immunofluorescence

Cells were fixed with 4% paraformaldehyde (PFA) in nuclease-free (NF) PBS for 15 min at room temperature, followed by permeabilization with 0.3% Triton X-100 in NF PBS for 10 min at room temperature. The cells were then washed twice with PBS and were prepared for immunofluorescence. The order of assays was always as follows: immunofluorescence followed by re-fixation for 15 min with 4% PFA in NF PBS at room temperature, followed by DNA FISH, followed by RNA FISH. The re-fixation post immunofluorescence is important to preserve the signals.

For immunofluorescence, cells were first blocked for non-specific binding using 1% NF BSA (Ambion) for 30 min at room temperature. Then the cells were incubated with the primary antibodies in 1% NF BSA for 60 min at room temperature. After two washes with NF PBS, the cells were incubated with the secondary antibodies in 1% NF BSA for 60 min at room temperature, followed by two washes with NF PBS.

For DNA FISH, cells were first washed with 2×NF SSC (Ambion, Thermo Fisher Scientific). After which the DNA was denatured with 70% formamide in 2×NF SSC at 80°C for 15 min. While DNA in the cells was being denatured, DNA hybridization mixture was prepared: 9 µl hybridization buffer (Empire Genomics)+1 µl probes. The mixture was heated at 80°C for 3 min to denature the probes. A slide was wiped clean with RNaseZap (Ambion, Thermo Fisher Scientific) and left to dry. After DNA denaturation, the DNA FISH hybridization mix was transferred to the slide, and the coverslip was placed over it carefully. The cells were then incubated for hybridization for more than 40 h at 37°C in a dark, heavily-humidified chamber. After hybridization the cells were washed once with 2×SSC at room temperature followed by two 10-min washes with 50% formamide in 2×NF SSC at 37°C.

For smFISH, cells were first rinsed with 2×NF SSC followed by two brief washes with 10% formamide in 2×NF SSC at room temperature. smFISH hybridization mix was prepared as follows: 9 µl hybridization buffer (Stellaris)+1 µl formamide+0.5 µl RNA FISH probes. The slides were wiped clean with RNaseZap and were allowed to dry completely. The hybridization mix was then transferred onto the slide and the coverslip was carefully placed over it. The cells were then incubated overnight at 37°C in a dark, heavily-humidified chamber. The next day, cells were washed once with 2×SSC at room temperature followed by two 5-min washes with 10% formamide in 2×NF SSC at 37°C. Finally, the cells were DNA stained with 1 µg/ml Hoechst 33342 dye for 10 min.

Antibodies, FISH probes and chemicals used

CCNA2 protein was labeled with a rabbit antibody (1:500) from Abcam (ab181591). For detection, goat anti-rabbit IgG antibody (1:500) with Alexa Fluor 647 dye was used. Pre-labeled *CCNA2* DNA FISH probes were procured from Empire Genomics (CCNA2-20-Re). The fluorophore was spectrally similar to Alexa Fluor 594. The hybridization buffer was supplied along with the probes.

For RNA smFISH the probes were designed using Stellaris Probe Designer by Biosearch technologies, and probes and hybridization buffer were ordered from the same source. The probes were labeled with Quasar 570 fluorophores. The probe sequences are available in Table S1 and have been described previously (Dhuppar and Mazumder, 2018).

Ambion ultrapure 50 mg/ml BSA (AM2616) was procured from Invitrogen. All other reagents (including PBS, SSC, water and RNaseZap) were Ambion RNase-free products from Invitrogen, Thermo Fisher Scientific.

Microscopy

Imaging was always performed with Vectashield as a mounting medium. Images were acquired at 14-bit resolution using a fully-automated Olympus IX83 microscope on a Retiga 6000 camera (QImaging). All images were take using a 60× oil objective with 1.42 NA. 31 planes with 300 nm step size were taken for every field. Appropriate filter cubes from Chroma Technologies (49309 ET – Orange#2 FISH and 49310 ET – Red#2 FISH) and Olympus were used to prevent any bleed through across the spectrum of fluorophores.

Image and data analysis

The 3D stacks were first average projected and analyzed for DNA content using an automated MATLAB (MathWorks) routine developed previously (Dhuppar and Mazumder, 2018). Thereafter, the 3D stack corresponding to each nucleus in the field was sent one-by-one to another module for texture-based removal of the out-of-focus light followed by 3D segmentation of the nucleus (Fig. 2). After segmentation, the boundary voxels and the centroid of each cell nucleus were used to find relevant distances. A closeness metric was defined for relative distances of the alleles from the lamina and the centroid thus: ratio of the distance of an allele from the centroid to the sum of the distances from the lamina and the centroid (Fig. 3). Its value lies always between 0 and 1: unity if the allele is on the lamina and zero if it is at the centroid. The 3D segmentation was done on a cell-by-cell basis to reduce the size of the images and hence make the computation feasible with a desktop computer.

For position-dependent analysis of gene expression, only nuclei with exactly three clearly identified copies of the *CCNA2* gene were used (446 cells) – they formed ∼73% of a total population of 611 cells.

The physical size of a pixel on the camera was 4.54 µm, corresponding to an area of 20.6 µm^2. Using a 60×1.42 NA objective without binning, this translates to 5.73×10^{-3} µm^2 on the sample. With stack separation of 300 nm, the voxel volume comes to 1.72×10^{-3} µm^3. Distances in 3D calculated found similarly. Images for the purpose of visualization were prepared using ImageJ (National Institutes of Health).

All image analyses were performed using MATLAB (MathWorks). For graphs, MATLAB and Python 3 were used. All code and programs used in this study are available on https://github.com/shuppar.

Acknowledgements
S.D. thanks Dr Sitara Roy for many useful suggestions on data representation and visualization.

Competing interests
The authors declare no competing or financial interests.

Author contributions
Conceptualization: S.D., A.M.; Methodology: S.D., A.M.; Software: S.D.; Validation: S.D.; Formal analysis: S.D.; Investigation: S.D., A.M.; Resources: S.D., A.M.; Data curation: S.D.; Writing - original draft: S.D., A.M.; Writing - review & editing: S.D., A.M.; Visualization: S.D., A.M.; Supervision: A.M.; Project administration: A.M.; Funding acquisition: A.M.

Funding
This project was funded by intramural funds at the Tata Institute of Fundamental Research Hyderabad from the Department of Atomic Energy, Government of India and partially funded by a DST Science and Engineering Research Board Early Career Research Award (ECR/2016/000907) to A.M.

Supplementary information
Supplementary information available online at
http://jcs.biologists.org/lookup/doi/10.1242/jcs.246330.supplemental

Peer review history
The peer review history is available online at
https://jcs.biologists.org/lookup/doi/10.1242/jcs.246330.reviewer-comments.pdf

References
Bienko, M., Crosetto, N., Teytelman, L., Klemm, S., Itzkovitz, S. and Van Oudenaarden, A. (2013). A versatile genome-scale PCR-based pipeline for high-definition DNA FISH. *Nat. Methods* **10**, 122-124. doi:10.1038/nmeth.2306

Bolland, D. J., King, M. R., Reik, W., Corcoran, A. E. and Krueger, C. (2013). Robust 3D DNA FISH using directly labeled probes. *J. Vis. Exp.* **78**, e50587. doi:10.3791/50587

Buxbaum, A. R., Haimovich, G. and Singer, R. H. (2015). In the right place at the right time: visualizing and understanding mRNA localization. *Nat. Rev. Mol. Cell Biol.* **16**, 95-109. doi:10.1038/nrm3918

Century, T. J., Fenichel, I. R. and Horowitz, S. B. (1970). The concentrations of water, sodium and potassium in the nucleus and cytoplasm of amphibian oocytes. *J. Cell Sci.* **7**, 5-13

Chambeyron, S. and Bickmore, W. A. (2004). Chromatin decondensation and nuclear reorganization of the HoxB locus upon induction of transcription. *Genes Dev.* **18**, 1119-1130. doi:10.1101/gad.292104

Clemson, C. M., Hutchinson, J. N., Sara, S. A., Ensminger, A. W., Fox, A. H., Chess, A. and Lawrence, J. B. (2009). An architectural role for a nuclear noncoding RNA: NEAT1 RNA is essential for the structure of paraspeckles. *Mol. Cell* **33**, 717-726. doi:10.1016/j.molcel.2009.01.026

Cooper, G. M. (2000). *The Cell: A Molecular Approach*: Sinauer Associates.

Cremer, T. and Cremer, C. (2001). Chromosome territories, nuclear architecture and gene regulation in mammalian cells. *Nat. Rev. Genet.* **2**, 292-301. doi:10.1038/35066075

Crick F. (1970). Central dogma of molecular biology. Nature **227**, 561-563. doi:10.1038/227561a0

Day, D. A. and Tuite, M. F. (1998). Post-transcriptional gene regulatory mechanisms in eukaryotes: an overview. *J. Endocrinol.* **157**, 361-371. doi:10.1677/joe.0.1570361

Dhuppar, S. and Mazumder, A. (2018). Measuring cell cycle-dependent DNA damage responses and p53 regulation on a cell-by-cell basis from image analysis. *Cell Cycle* **17**, 1358-1371. doi:10.1080/15384101.2018.1482136

Ernst, J., Kheradpour, P., Mikkelsen, T. S., Shoresh, N., Ward, L. D., Epstein, C. B., Zhang, X., Wang, L., Issner, R., Coyne, M. et al. (2011). Mapping and analysis of chromatin state dynamics in nine human cell types. *Nature* **473**, 43-49. doi:10.1038/nature09906

Finlan, L. E., Sproul, D., Thomson, I., Boyle, S., Kerr, E., Perry, P., Ylstra, B., Chubb, J. R. and Bickmore, W. A. (2008). Recruitment to the nuclear periphery can alter expression of genes in human cells. *PLoS Genet.* **4**, e1000039. doi:10.1371/journal.pgen.1000039

Finn, E. H. and Misteli, T. (2019). Molecular basis and biological function of variability in spatial genome organization. *Science* **365**, eaaw9498. doi:10.1126/science.aaw9498

Finn, E. H., Pegoraro, G., Brandão, H. B., Valton, A.-L., Oomen, M. E., Dekker, J., Mirny, L. and Misteli, T. (2019). Extensive heterogeneity and intrinsic variation in spatial genome organization. *Cell* **176**, 1502-1515.e10. doi:10.1016/j.cell.2019.01.020

Fullwood, M. J., Liu, M. H., Pan, Y. F., Liu, J., Xu, H., Mohamed, Y. B., Orlov, Y. L., Velkov, S., Ho, A., Mei, P. H. et al. (2009). An oestrogen-receptor-α-bound human chromatin interactome. *Nature* **462**, 58-64. doi:10.1038/nature08497

Gerlich, D., Beaudouin, J., Kalbfuss, B., Daigle, N., Eils, R. and Ellenberg, J. (2003). Global chromosome positions are transmitted through mitosis in mammalian cells. *Cell* **112**, 751-764. doi:10.1016/S0092-8674(03)00189-2

Hall, L. L., Byron, M., Sakai, K., Carrel, L., Willard, H. F. and Lawrence, J. B. (2002). An ectopic human XIST gene can induce chromosome inactivation in postdifferentiation human HT-1080 cells. *Proc. Natl. Acad. Sci. USA* **99**, 8677-8682. doi:10.1073/pnas.132468999

Hall, L. L., Carone, D. M., Gomez, A. V., Kolpa, H. J., Byron, M., Mehta, N., Fackelmayer, F. O. and Lawrence, J. B. (2014). Stable C0T-1 repeat RNA is abundant and is associated with euchromatic interphase chromosomes. *Cell* **156**, 907-919. doi:10.1016/j.cell.2014.01.042

Holwerda, S. and Laat, W. (2012). Chromatin loops, gene positioning, and gene expression. *Front. Genet.* **3**, 217. doi:10.3389/fgene.2012.00217

Jiang, J., Jing, Y., Cost, G. J., Chiang, J.-C., Kolpa, H. J., Cotton, A. M., Carone, D. M., Carone, B. R., Shivak, D. A., Guschin, D. Y. et al. (2013). Translating dosage compensation to trisomy 21. *Nature* **500**, 296-300. doi:10.1038/nature12394

Li, C., Cesbron, F., Oehler, M., Brunner, M. and Höfer, T. (2018). Frequency modulation of transcriptional bursting enables sensitive and rapid gene regulation. *Cell Syst.* **6**, 409-423.e11. doi:10.1016/j.cels.2018.01.012

Lomvardas, S., Barnea, G., Pisapia, D. J., Mendelsohn, M., Kirkland, J. and Axel, R. (2006). Interchromosomal interactions and olfactory receptor choice. *Cell* **126**, 403-413. doi:10.1016/j.cell.2006.06.035

Misteli, T. (2001). Protein dynamics: implications for nuclear architecture and gene expression. *Science* **291**, 843-847. doi:10.1126/science.291.5505.843

Misteli, T. (2005). Concepts in nuclear architecture. *Bioessays* **27**, 477-487. doi:10.1002/bies.20226

Monier, K., Armas, J. C. G., Etteldorf, S., Ghazal, P. and Sullivan, K. F. (2000). Annexation of the interchromosomal space during viral infection. *Nat. Cell Biol.* **2**, 661-665. doi:10.1038/35023615

Morey, C., Da Silva, N. R., Perry, P., Bickmore, W. A., Kanno, M., Taniguchi, M., Vidal, M., Alkema, M., Berns, A. and Koseki, H. (2007). Nuclear reorganisation and chromatin decondensation are conserved, but distinct, mechanisms linked to Hox gene activation. *Development* **134**, 909-919. doi:10.1242/dev.02779

Morey, C., Kress, C. and Bickmore, W. A. (2009). Lack of bystander activation shows that localization exterior to chromosome territories is not sufficient to up-regulate gene expression. *Genome Res.* **19**, 1184-1194. doi:10.1101/gr.089045.108

Nagano, T., Lubling, Y., Várnai, C., Dudley, C., Leung, W., Baran, Y., Mendelson Cohen, N., Wingett, S., Fraser, P. and Tanay, A. (2017). Cell-cycle dynamics of chromosomal organization at single-cell resolution. *Nature* **547**, 61-67. doi:10.1038/nature23001

Osborne, C. S., Chakalova, L., Brown, K. E., Carter, D., Horton, A., Debrand, E., Goyenechea, B., Mitchell, J. A., Lopes, S., Reik, W. et al. (2004). Active genes dynamically colocalize to shared sites of ongoing transcription. *Nat. Genet.* **36**, 1065-1071. doi:10.1038/ng1423

Osborne, C. S., Chakalova, L., Mitchell, J. A., Horton, A., Wood, A. L., Bolland, D. J., Corcoran, A. E. and Fraser, P. (2007). Myc dynamically and preferentially relocates to a transcription factory occupied by Igh. *PLoS Biol.* **5**, e192. doi:10.1371/journal.pbio.0050192

Pageau, G. J., Hall, L. L. and Lawrence, J. B. (2007). BRCA1 does not paint the inactive X to localize XIST RNA but may contribute to broad changes in cancer that impact XIST and Xi heterochromatin. *J. Cell. Biochem.* **100**, 835-850. doi:10.1002/jcb.21188

Parada, L. A., McQueen, P. G. and Misteli, T. (2004). Tissue-specific spatial organization of genomes. *Genome Biol.* **5**, R44. doi:10.1186/gb-2004-5-7-r44

Probst, A. V., Dunleavy, E. and Almouzni, G. (2009). Epigenetic inheritance during the cell cycle. *Nat. Rev. Mol. Cell Biol.* **10**, 192-206. doi:10.1038/nrm2640

Raj, A., Peskin, C. S., Tranchina, D., Vargas, D. Y. and Tyagi, S. (2006). Stochastic mRNA synthesis in mammalian cells. *PLoS Biol.* **4**, 1707-1719. doi:10.1371/journal.pbio.0040309

Raj, A., van den Bogaard, P., Rifkin, S. A., van Oudenaarden, A. and Tyagi, S. (2008). Imaging individual mRNA molecules using multiple singly labeled probes. *Nat. Methods* **5**, 877-879. doi:10.1038/nmeth.1253

Reddy, K. L., Zullo, J. M., Bertolino, E. and Singh, H. (2008). Transcriptional repression mediated by repositioning of genes to the nuclear lamina. *Nature* **452**, 243-247. doi:10.1038/nature06727

Sadasivam, S. and DeCaprio, J. A. (2013). The DREAM complex: master coordinator of cell cycle-dependent gene expression. *Nat. Rev. Cancer* **13**, 585-595. doi:10.1038/nrc3556

Sexton, T., Schober, H., Fraser, P. and Gasser, S. M. (2007). Gene regulation through nuclear organization. *Nat. Struct. Mol. Biol.* **14**, 1049-1055. doi:10.1038/nsmb1324

Stadhouders, R., Vidal, E., Serra, F., Di Stefano, B., Le Dily, F., Quilez, J., Gomez, A., Collombet, S., Berenguer, C., Cuartero, Y. et al. (2018). Transcription factors orchestrate dynamic interplay between genome topology and gene regulation during cell reprogramming. *Nat. Genet.* **50**, 238-249. doi:10.1038/s41588-017-0030-7

Stadhouders, R., Filion, G. J. and Graf, T. (2019). Transcription factors and 3D genome conformation in cell-fate decisions. *Nature* **569**, 345-354. doi:10.1038/s41586-019-1182-7

Thomson, I., Gilchrist, S., Bickmore, W. A. and Chubb, J. R. (2004). The radial positioning of chromatin is not inherited through mitosis but is established de novo in early G1. *Curr. Biol.* **14**, 166-172. doi:10.1016/j.cub.2003.12.024

Wang, H., Xu, X., Nguyen, C. M., Liu, Y., Gao, Y., Lin, X., Daley, T., Kipniss, N. H., La Russa, M. and Qi, L. S. (2018). CRISPR-mediated programmable 3D genome positioning and nuclear organization. *Cell* **175**, 1405-1417;e14. doi:10.1016/j.cell.2018.09.013

Wang, M., Zhang, J., Xu, H. and Golding, I. (2019). Measuring transcription at a single gene copy reveals hidden drivers of bacterial individuality. *Nat. Microbiol.* **4**, 2118-2127. doi:10.1038/s41564-019-0553-z

Wray, G. A., Hahn, M. W., Abouheif, E., Balhoff, J. P., Pizer, M., Rockman, M. V. and Romano, L. A. (2003). The evolution of transcriptional regulation in eukaryotes. *Mol. Biol. Evol.* **20**, 1377-1419. doi:10.1093/molbev/msg140

Zenklusen, D., Larson, D. R. and Singer, R. H. (2008). Single-RNA counting reveals alternative modes of gene expression in yeast. *Nat. Struct. Mol. Biol.* **15**, 1263-1271. doi:10.1038/nsmb.1514

Zhang, L.-F., Huynh, K. D. and Lee, J. T. (2007). Perinucleolar targeting of the inactive X during S phase: evidence for a role in the maintenance of silencing. *Cell* **129**, 693-706. doi:10.1016/j.cell.2007.03.036

Zhao, B. S., Roundtree, I. A. and He, C. (2017). Post-transcriptional gene regulation by mRNA modifications. *Nat. Rev. Mol. Cell Biol.* **18**, 31-42. doi:10.1038/nrm.2016.132